ACS APPLIED MATERIALS & INTERFACES

Research Article

www.acsami.org

Li Ion Dynamics along the Inner Surfaces of Layer-Structured 2H–Li_xNbS_2

B. Stanje,*[,†] V. Epp,[†] S. Nakhal,[‡] M. Lerch,[‡] and M. Wilkening[†]

[†]Christian Doppler Laboratory for Lithium Batteries, and Institute for Chemistry and Technology of Materials (Member of NAWI Graz), Graz University of Technology, Stremayrgasse 9, A-8010 Graz, Austria

[‡]Technische Universität Berlin, Institut für Chemie, Straße des 17. Juni 135, D-10623 Berlin, Germany

ABSTRACT: Layer-structured materials, such as graphite (LiC_y) or $Li_x(Co,Ni,Mn)O_2$, are important electrode materials in current battery research that still relies on insertion materials. This is due to their excellent ability to reversibly accommodate small alkali ions such as Li^+ and Na^+. Despite of these applications, microscopic information on Li ion self-diffusion in transition metal sulfides are relatively rare. Here, we used ^{7}Li nuclear magnetic resonance (NMR) spectroscopy to study translational Li ion diffusion in hexagonal (2H) Li_xNbS_2 (x = 0.3, 0.7, and 1) by means of variable-temperature NMR relaxometry. ^{7}Li spin–lattice relaxation rates and ^{7}Li NMR spectra were used to determine Li jump rates and activation barriers as a function of Li content. Hereby, NMR spin–lattice relaxation rates recorded with the spin-lock technique offered the possibility to study Li ion dynamics on both the short-range and long-range length scale. Information was extracted from complete diffusion-induced rate peaks that are obtained when the relaxation rate is plotted vs inverse temperature. The peak maximum of the three samples studied shifts toward higher temperatures with increasing Li content x in 2H–Li_xNbS_2. Information on the dimensionality of the diffusion process was experimentally obtained by *frequency dependent* R_ρ measurements carried out at T = 444 K, that is in the high-temperature regime of the rate peaks. A slight, but measurable frequency-dependence within this limit is found for all samples; it is in good agreement with predictions from relaxation models developed to approximate low-dimensional (2D) jump diffusion.

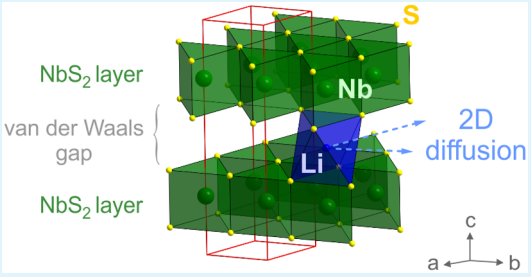

KEYWORDS: *NMR, relaxation, dimensionality, insertion materials, jump diffusion*

1. INTRODUCTION

The principle of lithium-ion[1,2] (or sodium-ion) batteries that use insertion compounds as electrode materials is based on the highly reversible accommodation of the ionic charge carriers. In the case of layered transition metal dichalcogenides (TMDs), titanium disulfide, TiS_2, belongs to one of the first anode materials whose topotactic reaction with lithium has been studied in detail. Still TMDs play an important role in battery technology;[2,3] in general, their chemical versatility as compared to graphene makes them fundamentally and technologically intriguing.[4−6] It has been shown that besides the composition and positioning of atoms in such materials, understanding the low dimensional diffusion processes, also in terms of jump rates and hopping barriers, is key to developing new electrode materials and those with tunable electronic properties.[7,8]

Recently, Goodenough and co-workers reinvestigated the electrochemical insertion behavior and battery performance of the intercalation hosts 2H-NbS_2 and 3R-NbS_2 and showed the usability of niobium disulfide as potential cathode material in secondary Li-ion batteries.[9,10] While usually the electrochemical properties of potential candidates are extensively evaluated, only few experimental studies take up the challenge to describe the underlying Li diffusion mechanisms in detail from an atomic scale point of view. Here, Li_xNbS_2 served as a low-dimensional model system for a comprehensive ^{7}Li NMR relaxation study to gain insight into the Li ion dynamics between the van der Waals gap of the NbS_2 sheets. In particular, activation energies (E_a) and Li correlation times (τ_c) have been determined. Besides NMR, also neutron scattering can be used to evaluate ion dynamics and diffusion pathways. In contrast to neutron scattering that, which is sensitive to ion dynamics with residence times on the ps time scale, NMR, however, is able to probe much slower ion dynamics. Using the appropriate NMR relaxation method, ion dynamics near ambient conditions can be probed as it is done here.

There are two different polytype hexagonal structures for niobium disulfide with different stacking order of the NbS_6 prisms known.[11−13] The first, 2H-NbS_2, is composed of two NbS_2 layers per unit cell (space group: $P6_3/mmc$) whereas the second one, 3R-NbS_2, consists of three layers per unit cell (space group: $R3m$) as shown in Figure 1.

Whereas the 2D Li self-diffusion process of the 3R modification was already studied by our group recently,[14] almost no NMR data could be found for the 2H modification. Here, we focused on the 2H polymorph and took advantage of variable-temperature ^{7}Li NMR relaxation measurements and

Received: November 17, 2014
Accepted: January 29, 2015
Published: January 29, 2015

DOI: 10.1021/am5078655
ACS Appl. Mater. Interfaces 2015, 7, 4089−4099

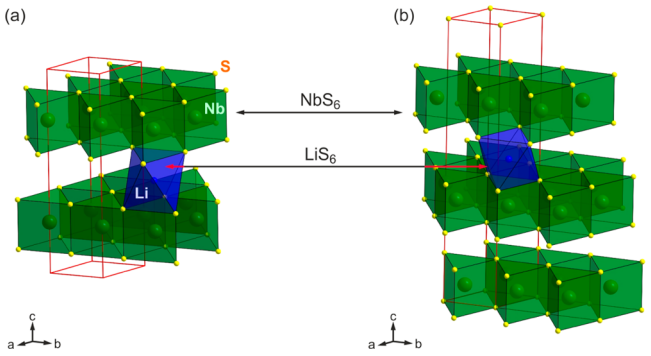

Figure 1. Crystal structures of (a) 2H-NbS_2 and (b) 3R-NbS_2 with LiS_6 octahedral sites (blue) and NbS_6 trigonal prismatic sites (green).[12,13]

line shape studies to collect information on ion dynamics of three fully homogenized samples with different Li contents, namely, 2H−Li_xNbS_2 with x = 0.3, 0.7, and 1. Spin−lattice relaxation measurements in both the laboratory (R_L) and rotating frame of reference (R_ρ) were carried out as a function of temperature to investigate short-range as well as long-range Li ion dynamics.[15] While the first are sensitive to ion hopping on the Ångström length scale, the latter is comparable to that usually probed via conductivity spectroscopy in the low frequency limit.[16] In particular, even if powder samples are used in NMR relaxometry, the method allows to deduce information on the dimensionality of the relevant diffusion process via frequency-dependent measurements.[17−24]

In the present study, we were able to precisely correlate the Li self-diffusion parameters with the change of the Li content x and the lattice parameters of the samples studied. We used chemically lithiated samples in order to avoid the influence of binders, conductive additives and the formation of passivation layers if Li insertion is carried out electrochemically. Additives usually needed to prepare electrodes might also influence the diffusion properties; regarding a similar study on $Li_4Ti_5O_{12}$ we do not expect significant differences for bulk properties.[25] This is, however, beyond the scope of the present study. Fortunately, since complete diffusion-induced relaxation rate peaks in the rotating frame of reference were accessible, we reached the so-called high-temperature flank of the corresponding rate peaks containing information on the dimensionality of the diffusion process.[23,26] The results were compared with predictions of NMR relaxation models developed for low-dimensional diffusion.[27]

2. EXPERIMENT

2H-NbS_2 was prepared by direct synthesis from the elements in an evacuated silica ampule. The ampule was heated at 400 °C for 10 days to achieve complete reaction of the elemental sulfur, afterward it was kept at 700 °C for 7 days. Chemical lithiation of 2H-NbS_2 was carried out by stirring the powder in a 2.5 M solution of *n*-butyllithium in hexane at room temperature for 7 days under dry nitrogen atmosphere. Subsequently, the samples were heated at 400 °C for homogenization, that is, Li ion distribution, in sealed quartz ampules for 1 week. Due to their air-sensitivity they were fire-sealed under vacuum in DURAN glass ampules (~4 cm in length and 0.5 cm in diameter) to permanently exclude moisture and air. The ampules were placed inside the NMR probe.

Prior to our NMR measurements the powders were chemically characterized by combustion analysis (Thermo Finnigan FlashEA 1112 NC analyzer) for hydrogen content. The amount of oxygen was determined using a LECO EF-TC 300 N_2/O_2 analyzer according to the hot gas extraction method. In addition, X-ray fluorescence analysis (PANalytical Axios PW4400/24 X-ray fluorescence spectrometer with an Rh-tube and wavelength dispersive detection) was used to check the niobium metal and sulfur content, respectively.

A PANalytical X'Pert PRO MPD diffractometer (Cu K_α radiation, Bragg−Brentano (θ−θ) geometry) with a PIXcel detector was used for the powder XRD measurements. The program package FULL PROF 2006 was used for structural refinements.[28] The reflection profiles were fitted with a pseudoVoigt function.

^{7}Li NMR measurements were performed using a Bruker Avance III spectrometer connected to a shimmed cryo-magnet B_0 = 7.04 T with a nominal ^{7}Li resonance frequency of $\omega_0/2\pi$ = 116.4 MHz. A ceramic high-temperature NMR probe (Bruker BioSpin) was used that allows $\pi/2$ pulse lengths of about 6 to 7.5 μs at 200 W. The temperatures, adjusted via a Eurotherm controller and a stream of N_2 gas, ranged from 223 to 573 K.

Variable-temperature ^{7}Li NMR spectra and ^{7}Li spin−lattice relaxation NMR rates ($1/T_1 = R_1$) in the laboratory frame of reference were acquired under static, i.e., nonrotating conditions. R_1 rates were recorded with the saturation recovery pulse sequence ($10 \times \pi/2 - t_d - \pi/2$−acquisition (acq.)).[29] The initial sequence of ten $\pi/2$ pulses was used to destroy any longitudinal magnetization M_z. Then, the recovery of $M_z(t_d)$ was recorded after the final $\pi/2$ pulse as a function of the delay time t_d. While Li diffusion is expected to govern longitudinal recovery in Li_xNbS_2 at sufficiently high temperatures,

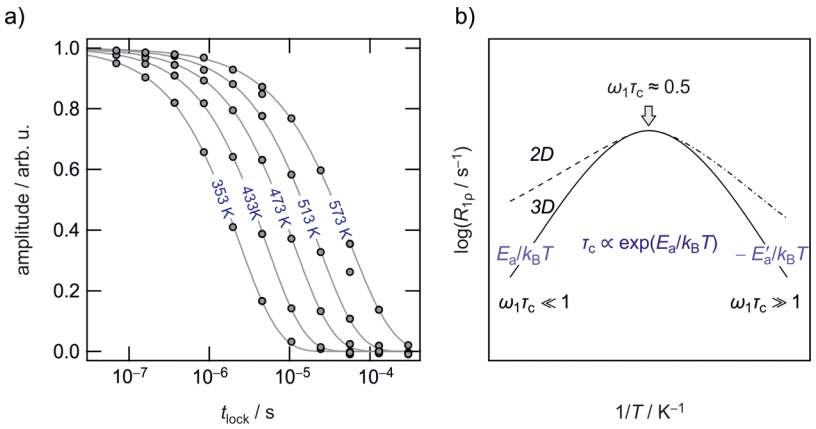

Figure 2. (a) ^{7}Li transversal decay of the spin-locked magnetization $M_\rho(t_{lock})$ recorded at the temperatures indicated ($\omega_1/2\pi$ = 20 kHz). The solid lines represent fits according to stretched exponentials yielding the parameters $R_{1\rho}$ and γ'; note that the x-axis is scaled logarithmically. (b) Schematic representation of the diffusion induced NMR $R_{1\rho}$ rate peaks.

DOI: 10.1021/am5078655
ACS Appl. Mater. Interfaces 2015, 7, 4089−4099

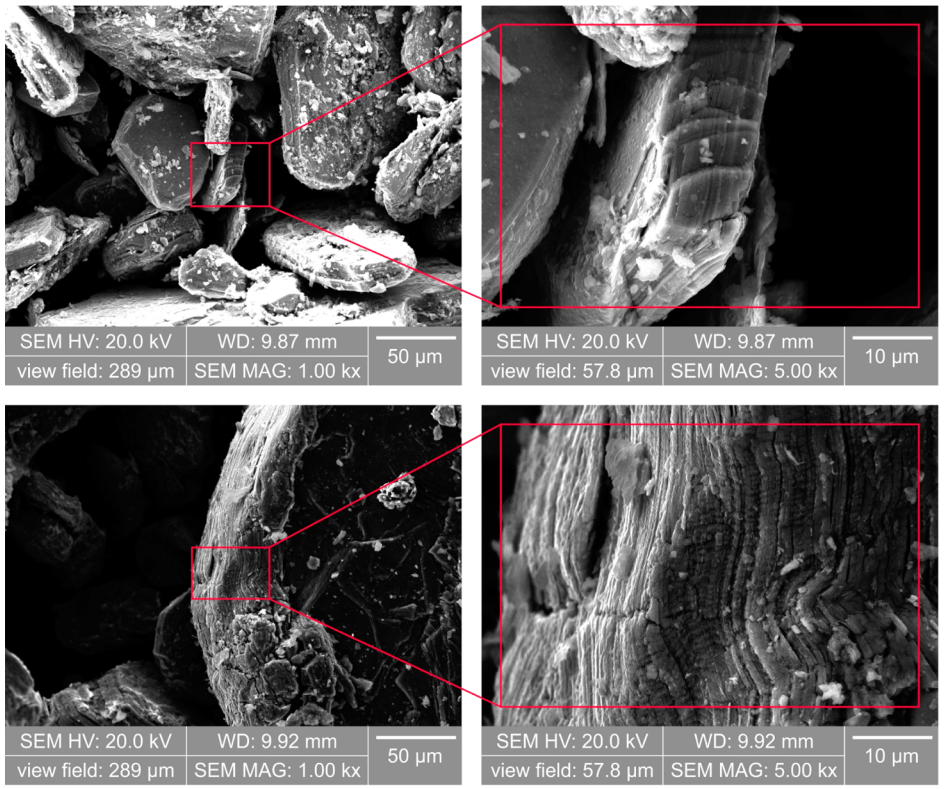

Figure 3. SEM images of powdered 2H−Li_xNbS_2 (after Li insertion, $x = 0.7$). Red squares indicate a zoom into the rectangular area marked on the left.

nondiffusive recovery because of lattice vibrations or coupling to conduction electrons will influence the R_1 rates at lower temperatures.

^{7}Li spin−lattice relaxation NMR rates in the rotating frame of reference ($1/T_{1\rho} = R_{1\rho}$) were recorded by using the spin-locking technique ($\pi/2_{x'}$ − spin locking pulse (t_{lock}) − acq.) at an angular locking frequency $\omega_1/2\pi$ of ∼20 kHz.[29−32] This technique is sensitive to much slower Li diffusion processes compared to R_1 NMR measurements in the lab frame. First, the equilibrium magnetization M_z is flipped onto the y' axis by applying a $\pi/2_{x'}$ pulse along the x' axis. The pulse is followed by a 90° phase-shifted locking pulse being in parallel to the resulting magnetization vector $M_{y'}$. The corresponding magnetic B_1 field formerly replaces the external one B_0 and represents a new reference point for spin relaxation. The initial, transversal magnetization has to adapt itself to the much smaller B_1 field. Accordingly, a transversal decay of the amplitude of the $M_{y'}$ vector can be observed. After switching off the locking pulse, $M_{y'}$ (= M_ρ) is measured as a function of the duration of the spin-lock t_{lock} pulse by recording the resulting FID. The longer the locking pulse, the smaller the amplitude of the $M_{y'}$ vector. Here, the R_ρ rates $R_{1\rho}$ at the given locking frequency were obtained from the transversal transients recorded by varying the duration of t_{lock} from 30 μs to 300 ms. The recycle delay for R_ρ measurements was at least 5 times T_1. R_1 and $R_{1\rho}$ were obtained by parametrizing the resulting magnetic transients $M_z(t_d)$ and $M_\rho(t_{lock})$, respectively, by stretched exponentials of the form $M_z(t_d) \propto 1-\exp[-(t_d/T_1)^\gamma]$ and $M_\rho(t_{lock}) \propto \exp[-(t_{lock}/T_{1\rho})^{\gamma'}]$ with the stretching exponents, γ and γ', ranging from 0.7 to 1.0, respectively (cf. Figure 2a) for some selected $R_{1\rho}$ transients).

3. BASICS OF NMR RELAXOMETRY

Fortunately, via the temperature-variable NMR SLR measurements described above we were able to record so-called diffusion-induced rate peaks from which activation energies and jump rates can be deduced. In addition, frequency-dependent NMR R_ρ rates were recorded at fixed temperature (444 K) on the high-T flank of the diffusion-induced rate peaks (see Figure 2b). In this T range the condition $\omega_1\tau_c \ll 1$ approximately holds. The locking frequency $\omega_1/2\pi$ was varied in from 5 to 20 kHz. While the peak maximum, for which the relation $\omega_1\tau_c \approx 0.5$ holds, can be used to extract the correlation time τ_c if $\omega_1/2\pi$ is known, the flanks yield the activation energies E_a and E_a'. Here, E_a' is usually influenced by correlation effects whereas E_a, if directly extracted from the slope of the flank, can be identified with the long-range activation energy provided a 3D diffusion process is given.[23,33−35] For 1D and 2D diffusion a relaxation model has to be used to deduce E_a from the relaxation peak.[27,30−32]

In Figure 2b, a diffusion induced rate peak is plotted against the inverse temperature indicating the maximum condition (indicated by an arrow) as well as the low-temperature and high-temperature limits. Only for uncorrelated, 3D isotropic diffusion $E_a' = E_a$ applies yielding a fully symmetric rate peak.[36] If correlation effects influence short-range ion hopping (see the dashed-dotted line), E_a' becomes smaller than E_a; both values are linked via $E_a'^{3D} = E_a^{3D} \times (\beta - 1)$ while β ($1 < \beta \leq 2$) denotes the frequency dependence of R_1 in the low-T limit. The parameter β, which has been introduced by Küchler et al.,[37] describes any asymmetry of the rate peak $R_{1\rho}$ caused by correlation effects in the low-T limit. Simultaneously, it is also a measure of the asymmetry of the rate peaks.[23] The activation energy $E_a^{2D,slope}$, which can be obtained from the slope of the rate in the limit $\omega_1\tau_c \gg 1$ (see dashed line), is linked with E_a^{2D} via $E_a^{2D,slope} = 0.75 \times E_a^{2D}$, provided β equals 2.[38]

4. RESULTS AND DISCUSSION

4.1. Crystal Structure and Morphology of 2H−Li_xNbS_2.

Before we present the results on spin−lattice relaxation NMR we would like to draw the reader's attention to the crystal

DOI: 10.1021/am5078655
ACS Appl. Mater. Interfaces 2015, 7, 4089−4099

structure and morphology of the Li_xNbS_2 samples studied and to the results from temperature-variable line shape measurements. NMR motional line narrowing (MN) gives first insights into how fast the ions are exchanged via self-diffusion among the crystallographic sites occupied.

In 2H-NbS_2 the niobium atoms occupy trigonal prismatic voids formed by the sulfur anions; each NbS_2 site shares edges with six nearest NbS_2 neighbors. In this structure lithium ions can be intercalated into the empty octahedral voids located in the van der Waals gap between the NbS_2 sheets. Li-centered octahedra stack along the *c* axis and alternate with layers of NbS_2. In the 2H polymorph each LiS_6 octahedra shares two common faces with an NbS_6 prism. This is different for the 3R form where the Li ions are located between an NbS_6 prism and an empty prism. Because of this difference, distinct diffusion pathways for the Li ions might be expected.

Morphology as Seen via SEM. The morphology and particle size of 2H−Li_xNbS_2 is presented in Figure 3 showing SEM images of the intercalated sample with $x = 0.7$. Large particles with a plate-like texture and a mean diameter of ca. 13 μm were found. In contrast to the synthesis starting from Li_2S, elemental niobium and Sulfur as reported by Goodenough and coworkers, chemical intercalation of Li ions in NbS_2 with *n*-butyllithium, as it is done here, results in no bouquet-like agglomerates of the primary particles as was observed recently.[10] The SEM images resemble that of nonlithiated 2H-NbS_2; this indicates that the Li has been inserted into the van der Waals gap between the NbS_2 layers without noticeable structural change of the intercalation host.[39] As is visible in the enlargements of the SEM pictures (see Figure 3, right) each larger primary particle consists of several layers of Li_xNbS_2.

Powder X-ray diffraction. Phase purity of the Li_xNbS_2 samples with $x = 0.3$, 0.7, and 1 was checked by powder X-ray diffraction carried out at room temperature (see Figures 4 and 5). The refined structural parameters and coordinates of the three samples investigated are listed in Tables 1 and 2.

As shown by Salyer et al.,[12] the lattice parameter *c* increases strongly with increasing lithium content for $x = 0$ to $x \approx 0.5$. For larger amounts of *x* the *c* parameter increases slightly with *x*. Our refined lattice parameters are in good agreement with values reported by Omloo and Jellinek.[38] Both the *a* and *c* lattice parameters of $Li_{0.7}NbS_2$ are slightly smaller than those reported by Salyer obtained from X-ray diffraction measurements of a single crystal.[16] A detailed investigation of lattice parameter variation with nominal composition for Li_xNbS_2 is already presented in ref 12, together with a detailed discussion of the behavior observed.

4.2. Static ^{7}Li NMR Spectra, Motional Narrowing. Temperature-variable NMR line shape measurements allow getting first insights into the jump processes of Li ions in solids in a relatively easy way. Here, all of the static ^{7}Li NMR spectra were recorded at various temperatures at a resonance frequency of 116.4 MHz. Independent of *x*, at lower temperatures (see Figure 6a) the spectra are composed of a single Gaussian shaped and slightly asymmetric central line with widths (full width at half-maximum, fwhm) ranging from 6.2 kHz ($x = 0.3$) up to 7.7 kHz ($x = 0.7$); considering the shape no distinct differences are seen. At the bottom of the lines tails of a quadrupole powder pattern are visible. This is due to the electric quadrupole interaction of the quadrupole moment of Li (spin-3/2) with a nonvanishing electric field gradient (EFG) at the Li site in Li_xNbS_2.[40] The interaction, which can be described by first order perturbation theory for ^{7}Li, alters the Zeeman levels leading to three different spin transitions.[40]

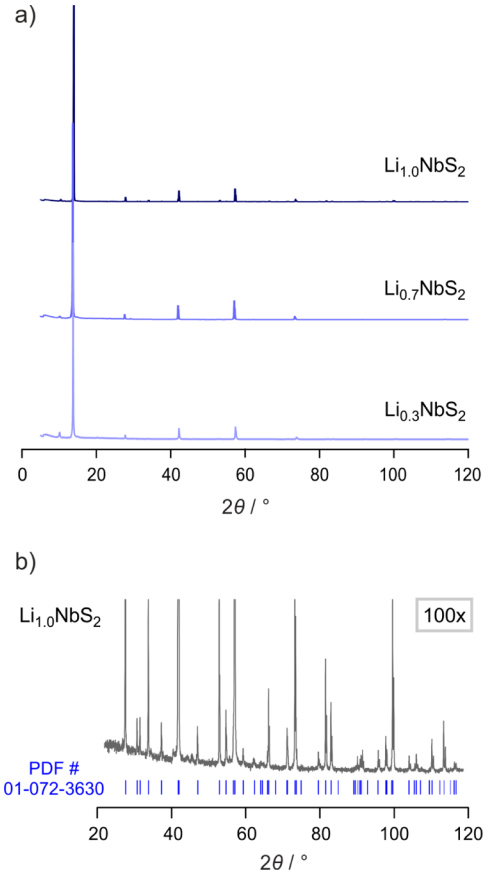

Figure 4. (a) Normalized X-ray powder diffractograms of the three samples investigated. For the sake of clarity, the larger reflections are reduced in their intensity. The patterns recorded indicate Li_xNbS_2 with high purity. (b) Magnification of the low-intensity reflections of the XRD pattern of $Li_{1.0}NbS_2$. Vertical bars indicate the positions of reflections expected for Li_xNbS_2.

In Figure 6b, spectra are presented that were measured at $T = 475$ K. With increasing *T* the central line, which is dipolarly broadened at low *T*, transforms into a Lorentzian shaped and asymmetric signal. Since dipole−dipole interactions are averaged due to rapid Li exchange with values in the kHz range, now a well visible quadrupole pattern shows up with sharp 90° singularities. For 2H−Li_xNbS_2 with $x = 1$ we observe a single quadrupole pattern indicating a single set of electrically equivalent Li positions.[40,41] If we assume axially symmetric EFGs, from the fully developed quadrupole powder pattern (410 K), which starts to emerge at $T > 330$ K, C_Q (^{7}Li, 384 K) $\approx$ 17 kHz can be easily estimated from the frequency distance $\Delta\nu_Q$ between the most intense satellite lines.

In contrast to $Li_{1.0}NbS_2$, the spectra of the samples with an intercalation degree of $x = 0.3$ and 0.7, respectively, indicate the presence of more than one inequivalent Li position occupied. For the sample with $x = 0.7$ besides the main pattern with C_{Q1}(^{7}Li, 413 K) $\approx$ 16.5 kHz (see Figure 6b) another set of singularities with very low intensity shows up that is characterized by C_{Q2}(^{7}Li, 384 K) $\approx$ 7.2 kHz. For $x = 0.3$ we obtain C_Q(^{7}Li, 413 K) $\approx$ 11 kHz. Obviously, at intermediate values of *x* the Li ions have access to more than one crystallographic position in 2H-NbS_2. In agreement with two sets of quadrupole powder patterns, the line of $Li_{0.7}NbS_2$ (see

DOI: 10.1021/am5078655
ACS Appl. Mater. Interfaces 2015, 7, 4089−4099

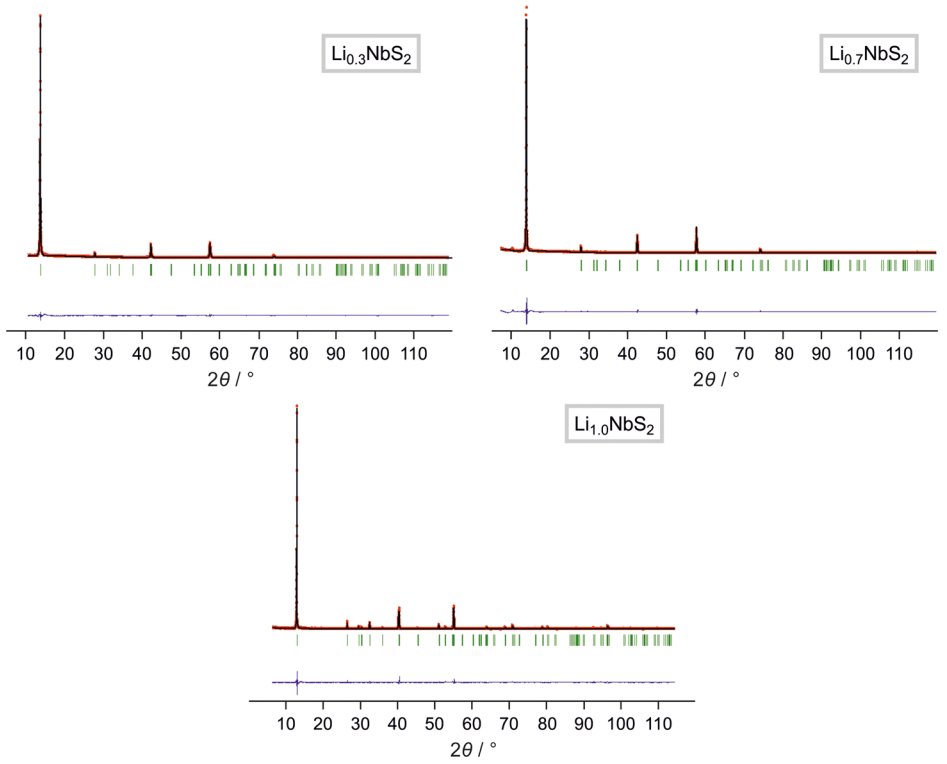

Figure 5. X-ray powder diagrams of $Li_{0.3}NbS_2$ (left), $Li_{0.7}NbS_2$ (right), and $Li_{1.0}NbS_2$ (bottom) with the results of the Rietveld refinements.

Table 1. Refined Structural Parameters for Li_xNbS_2 with x = 0.3, 0.7, and 1.0 at Ambient Temperature

	x =1.0	x = 0.7	x = 0.3
space group	$P6_3/mmc$	$P6_3/mmc$	$P6_3/mmc$
lattice parameter	a = 335.300 (8) pm	a = 334.03 (5) pm	a = 333.080 (14) pm
	c = 1290.23 (2) pm	c = 1288.02 (3) pm	c = 1281.79(2) pm
unit cell volume	V = 125.622(4) × 10^6 pm^3	V = 124.46(3) × 10^6 pm^3	V = 123.153(7) × 10^6 pm^3
formula units	Z = 2	Z = 2	Z = 2
2θ range	5−120°	5−120°	5−120°
R_{wp}	0.0688	0.0704	0.0546
R_{Bragg}	0.0606	0.0213	0.0213
R_{exp}	0.0266	0.0264	0.0266
S	2.58	2.66	2.05

Table 2. Refined Atomic Coordinates for Li_xNbS_2 with x = 0.3, 0.7, and 1.0 at Ambient Temperature

atom	Wyck. site	x	y	z[a]	occ. for $Li_{1.0}NbS_2$	occ. for $Li_{0.7}NbS_2$	occ. for $Li_{0.3}NbS_2$
Li	2*a*	0	0	0	0.08333	0.05833	0.025
Nb	2*b*	0	0	0.25	0.08333	0.08333	0.08333
S	4*f*	1/3	2/3	z	0.16666	0.16666	0.16666

[a] z = 0.12514(9) in $Li_{0.3}NbS_2$; z = 0.12520(12) in $Li_{0.7}NbS_2$; z = 0.12546(13) in $Li_{1.0}NbS_2$.

Figure 6b) also reveals a second central line that is characterized by its own chemical shift value. This feature is also seen for x = 0.3. We anticipate, however, that mainly the octahedral voids in the van der Waals gap are occupied, note that the intensity of the powder pattern leading to C_{Q2} (x = 0.7) is much weaker than that associated with C_{Q1}.

Independent of x, the central lines with the largest intensity show the typical asymmetry as expected for Li spins exposed to a spatially confined environment,[42] which is found in layer structured materials. The change of the corresponding quadrupole coupling constant from 11 kHz (x = 0.3) to 16.5 kHz (x = 0.7) and 17 kHz (x = 1) observed resembles the variation in the lattice constant c, see Table 1.

The change of the shape of the ^{7}Li NMR spectra over the temperature range covered here is illustrated in Figure 7, which presents exemplarily the line shapes of 2H−$Li_{1.0}NbS_2$. The spectra meet the expectations for a pure $Li_{1.0}NbS_2$ phase with the Li ions located inside the van der Waals gap. The fact that there is no averaging of the quadrupole intensities seen indicates spatially confined (two-dimensional) Li diffusion between the NbS_2 sheets; thus, this diffusion process is restricted to an exchange process between the electrically equivalent Li sites (2a) in the van der Waals gap of NbS_2.[42]

To collect quantitative information on Li ion dynamics, in Figure 6c the line width of the central transition was plotted vs temperature. Here, we focus on the most intense central line associated with the largest quadrupole powder pattern. The asymmetry is a clear indication of NMR chemical anisotropy being due to the layered structure of the material; similarly, this has been observed for Li_xTiS_2 by the NMR study of Prigge et al.[42] At T = 420 K it has already reached its full narrowing,

DOI: 10.1021/am5078655
ACS Appl. Mater. Interfaces 2015, 7, 4089−4099

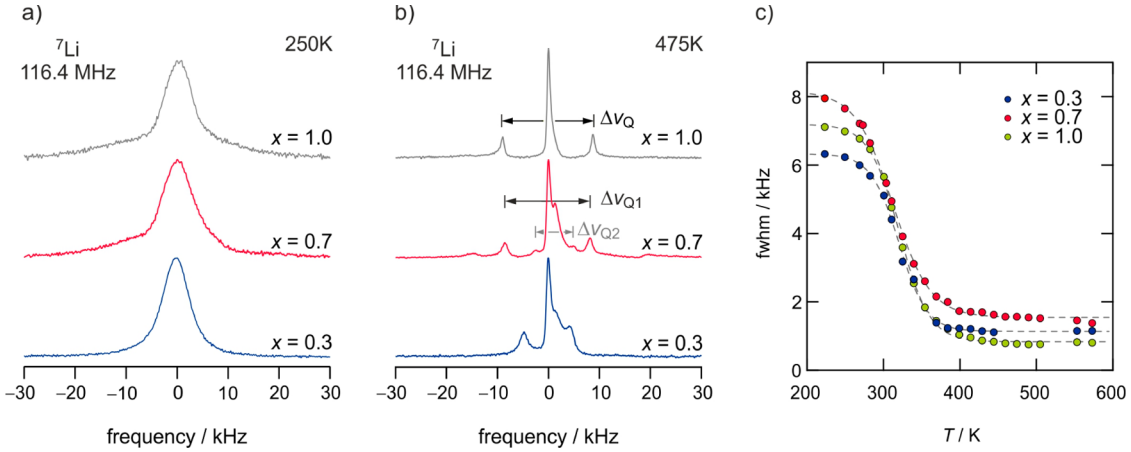

Figure 6. (a) ^{7}Li NMR spectra of annealed (that is, homogenized) layer-structured 2H–Li_xNbS_2 (x = 0.3, 0.7, and 1.0) recorded at $\omega_0/2\pi$ = 116.4 MHz and 250 K. See text for further explanation. (b) ^{7}Li NMR spectra of the samples shown in (a) but recorded at T = 475 K. (c) ^{7}Li NMR line width (full width at half-maximum, fwhm) as a function of temperature T. The dashed lines are to guide the eye.

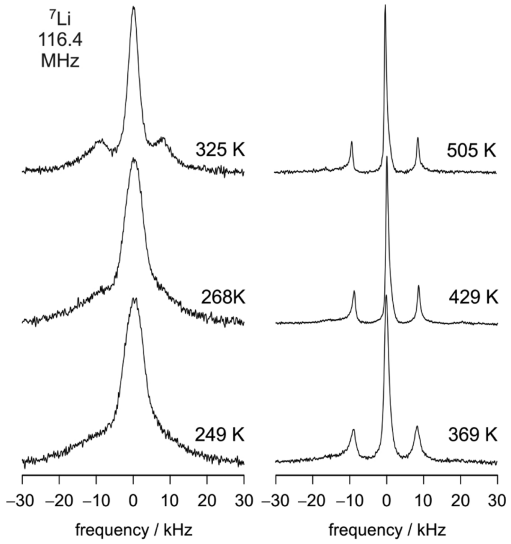

Figure 7. ^{7}Li NMR spectra of 2H–$Li_{1.0}NbS_2$ recorded at the temperatures indicated. With increasing T the line width of the central line, which is slightly anisotropic, undergoes a motional narrowing due to averaging of (homonuclear) ^{7}Li dipole–dipole interactions. At T > 320 K, a distinct quadrupole pattern appears that is fully developed at T > 420 K. By using a Hahn echo that overcomes dead-time receiver effects, the powder pattern can be enhanced in intensity.

therefore, the contribution of the second line was not taken into account to construct the MN curves. The fwhm was read off manually; no fitting functions were used because of the observed chemical shift asymmetry. The line width in the rigid lattice regime, $\nu_{rl}(x)$, depends on x; it takes a value of 7.9 kHz for x = 0.7 and 6.3 kHz for x = 1, respectively. The rigid lattice regime is reached at approximately 230 K.

Independent of Li content, the sulfides undergo a pronounced motional narrowing with increasing temperature due to increasing Li motions that are responsible for averaging of homonuclear dipole–dipole (^{7}Li–^{7}Li) interactions.[43] When the jump rate τ_{MN}^{-1} reaches the order of the rigid lattice line width notable diffusion-controlled line narrowing is expected. Here, narrowing sets in at approximately 260 K. The Li ion jump rate τ_{MN}^{-1} can be roughly estimated from the inflection point at approximately 320 K of the MN curves for all three samples according to $\tau_{MN}^{-1} \approx 2\pi \times \nu_{rl}$. For all three samples the Li jump rates τ_{MN}^{-1} turn out to be in the order of ~5 × 10^4 s^{-1}. Quite interestingly, although the intercalation degree x has been increased from x = 0.3 up to x = 1, no significant shift of the onset of motional narrowing is observed (see Figure 6c). Clear distinctions in Li diffusivity, however, can be revealed by R_ρ NMR as is shown below. NMR line narrowing seems to be less sensitive to the differences that can be observed with the spin-lock technique.

At first glance, we would expect that $\nu_{rl}(x)$ increases with x because of increasing homonuclear dipole–dipole interactions as is quantified by the van Vleck formalism.[40] Here, however, the change in lattice constant c, which is the largest for x = 1, likely leads to a smaller rigid-lattice line width for $Li_{1.0}NbS_2$ than expected.

4.3. ^{7}Li NMR Spin–Lattice Relaxation Measurements, Frequency Dependence, 2D Diffusion. To study Li diffusion parameters in more detail we measured both ^{7}Li R_1 and R_ρ/R rates at a Larmor frequency of $\omega_0/2\pi$ = 116.4 MHz and a locking frequency of 20 kHz (223 and 573 K), see refs 29 and 44–46 for an introduction into the basics of spin-lock measurements. In Figure 8 the rates $R_1(1/T)$ and $R_{1\rho}(1/T)$ together with the corresponding stretching exponents $\gamma(R_{1\rho})$ of the transients analyzed (see Figure 2) are shown in an Arrhenius plot.[47]

Whereas the R_1 transients $M_z(t_d)$ can be best represented with exponential functions (see the equation mentioned above), the corresponding magnetization curves and $M_\rho(t_{lock})$ need to be parametrized with $M_\rho(t_{lock}) \propto \exp[-(t_{lock}/T_{1\rho})^{\gamma'}]$ (see above) with γ' ranging between 0.7 and 1.0. The exact physical meaning of the stretching exponents is, in general, very difficult to explain; admittedly, in many cases no clear interpretation can be given. It is expected to be related to the shape of the underlying motional correlation function. In our opinion, intrinsic or extrinsic origins have to be considered: An intrinsically nonexponential motional correlation function might be expected for, for example, low-dimensional diffusion. Frequently, nonexponential decay behavior is related to a distribution of correlation rates being the direct consequence of a distribution of hopping barriers the ions have to overcome. Such extrinsic conditions would result in a superposition of distinct functions finally producing a stretched magnetization transient whose shape might change with temperature. In the

DOI: 10.1021/am5078655
ACS Appl. Mater. Interfaces 2015, 7, 4089–4099

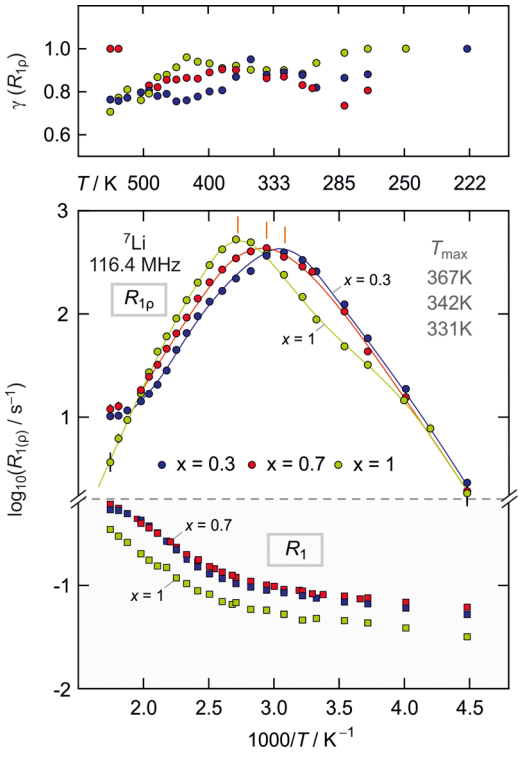

Figure 8. Arrhenius plot of the ^{7}Li NMR R_1 rates of 2H−Li$_x$NbS$_2$ recorded in the laboratory frame (R_1 (■), see bottom part of the figure) and in the rotating frame of reference ($R_{1\rho}$ (●), see upper part of the figure) measured at $\omega_0/2\pi$ = 116.4 MHz and at $\omega_1/2\pi$ = 20 kHz. The colors (see key) refer to the intercalation degree x of the samples (x = 0.3 (blue), x = 0.7 (red), and x = 1 (green)). The upper graph shows the dependence of the stretching exponents $\gamma(R_{1\rho})$ on T; the error margins of the exponents range from 0.1 to 0.2.

case of ^{7}Li, being a quadrupole nucleus, the interaction of its quadrupole moment with EFGs is expected to give complex nonexponential transients,[48] especially in the case of $R_{1\rho}$. Additionally, the latter are characterized by $\gamma' = 0.5$ if induced by the interactions of Li spins with paramagnetic centers.[49] Thus, there are various reasons that lead to the observation of stretched exponentials. Since no large change of γ' is observed in the present case, error margins are within ±0.2, and since many of the values range from 0.8 to 1.0, the stretched transients most likely reflect Li diffusion in a relatively regular potential landscape as it has been observed for Li$_{x=0.7}$TiS$_2$.[50] In particular, this holds for the sample with x = 0.3 (β = 1.8, see below), for which very similar activation energies are derived from R_1 and $R_{1\rho}$.

Coming back to the rates extracted from the transients measured, below approximately 300 K the rates R_1 are influenced by nondiffusive effects rather than by Li jump diffusion; at very low temperatures background relaxation is present that does only weakly depend on T. The corresponding relaxation rate ($R_{1,nd}$) is presumed to be caused by coupling of the Li spins with conduction electrons, paramagnetic impurities and/or by lattice vibrations. To separate its influence on the purely diffusion-induced relaxation, which shows up at elevated T, an empirical power law,

$$R_{1,nd} \propto T^{\kappa} \quad (1)$$

was used to extrapolate the background rates toward higher temperatures. With increasing T the rates R_1 pass into the low-T flank of a diffusion-induced rate peak. The high-T side, however, could not be reached since our NMR setup allows measurements up to 580 K only. For Li$_{0.3}$NbS$_2$, however, the rates seem to approach a maximum value at ∼570 K; compared to the other two samples this is a first indication that Li diffusivity in Li$_{0.3}$NbS$_2$ is faster than that for x = 0.7 and x = 1.0.

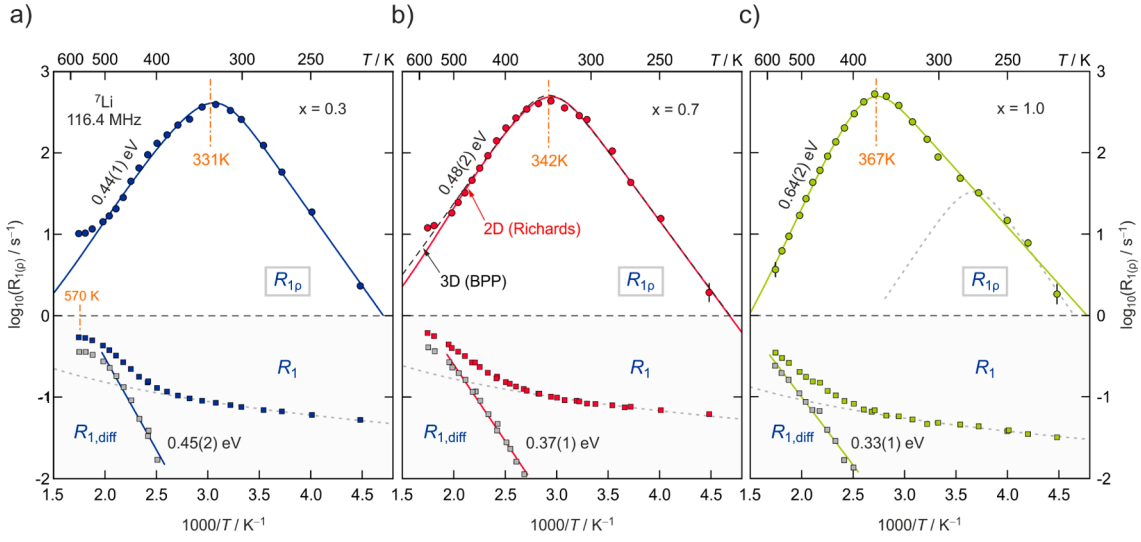

Figure 9. (a, b, and c) Detailed view of Arrhenius plot of the ^{7}Li NMR R_ρ rates of 2H−Li$_x$NbS$_2$ recorded at 166.4 MHz; the locking frequency set was 20 kHz. Solid lines show fits with an NMR model taking the 2D diffusion into account. The dashed line in panel (b) represents a modified BPP fit. Activation energies are obtained from the fits and are linked to long-range diffusion. Short-range activation energies $E_a'^{2D}$ were calculated using $E_a'^{2D} = E_a^{2D} \times (\beta - 1)$ where E_a^{2D} denotes the activation energy obtained from the fits according to the model of Richards.[27] They are in agreement with those values that can directly be obtained from the slopes of the low-T flanks (see text for further information). In order to obtain the purely diffusion-induced rates $R_{1,diff}$, nondiffusive background effects showing up at lower T have been taken into account by using an appropriate power law $R_{1,nd} \propto T^{\kappa}$ (with $\kappa_{x=0.3}$ = 1.34(1), see panel (a), $\kappa_{x=0.7}$ = 1.88(1), see pabel (b), and $\kappa_{x=1}$ = 1.27(8), see panel (c), represented by gray dashed lines). $R_{1,diff}$ values were obtained by subtraction $R_{1,nd}$ from the overall rates. Activation energies $E_{a,diff}$ were calculated from the slope of the linear fits shown (cf. the solid lines in the lower parts of the figures).

DOI: 10.1021/am5078655
ACS Appl. Mater. Interfaces 2015, 7, 4089−4099

In Figure 9a–c, the $R_1(1/T)$ as well as $R_{1,\mathrm{diff}}(1/T)$ are shown, which have been calculated according to[50]

$$R_1 = R_{1,\mathrm{diff}} + R_{1,\mathrm{nd}} \quad (2)$$

A fit according to eq 1 is also presented in Figure 9 yielding $\kappa = 1.34(1)$ for $x = 0.3$, $\kappa = 1.88(1)$ for $x = 0.7$, and $\kappa = 1.27(8)$ for $x = 1$. The purely diffusion-induced rates $R_{1,\mathrm{diff}}$ are represented by gray squares. The activation energies $E'_{a,\mathrm{diff}}$ were obtained from the slope of a linear fit of the corrected rates. Since R_1 (and so $R_{1,\mathrm{diff}}$) varies only slightly with T, the influence of $R_{1,\mathrm{nd}}$ is rather large resulting in activation energies that should be regarded as rough values. Here, we found 0.45(2) eV for $x = 0.3$; 0.37(1) eV for $x = 0.7$ and 0.33(1) eV for $x = 1$. $E'_{a,\mathrm{diff}}$, since it has been deduced in the limit $\omega_1\tau_c \gg 1$, is usually ascribed to short-range Li diffusion that is, in general, influenced by correlation effects such as Coulomb interactions and/or structural disorder.[23] Long-range ion dynamics, on the other hand, can only be inferred from the high-temperature flank of a diffusion-induced rate peak.[34,35] The intercalation degree x seems to have an impact on the activation energies characterizing short-range Li ion diffusion; the energies decrease from 0.45(2) eV for $x = 0.3$ to 0.33(1) eV for $x = 1$.

In our case, complete relaxation rate peaks can be obtained if the spins relax in a magnetic field B_1, the spin-lock field, that is much lower than the external one characterized by 116 MHz. In the upper part of the Arrhenius plot that is shown in Figure 8 the NMR R_ρ rates obtained are presented. The rates $R_{1\rho}$ pass through well-defined maxima showing up at different temperatures $T_{\max}$. In contrast to R_1 (as well as to the line widths measurements, vide supra), the $R_{1\rho}$ data do reveal a clear influence of the intercalation degree x on Li diffusivity, that is, the position of the rate maximum on the $1/T$ scale. According to the maximum condition, $\omega_1\tau_c \approx 0.5$, which is generally valid, the more the respective rate peak is shifted toward lower T, the higher the Li diffusivity. The latter is directly expressed by the correlation rate τ_c^{-1} being in the same order of magnitude as the Li jump rate τ^{-1}. Here, the highest diffusivity is found for the sample with $x = 0.3$ (see Figure 8). Note that the $R_{1\rho}$ rates follow a clear trend for $x = 0.3$, 0.7, and 1 which corroborates the above-mentioned indication of a R_1 peak maximum in the case of 2H–$Li_{0.3}NbS_2$. The temperatures $T_{\max}$ are as follows: 331 K for $x = 0.3$, 342 K for $x = 0.7$ and 367 K for $x = 1$. Inserting $\omega_1/2\pi = 20$ kHz, τ_c^{-1} is given by $\tau_c^{-1} \approx \tau_{(\rho)}^{-1} = 3 \times 10^5\ \mathrm{s}^{-1}$ at $T_{\max}$. This value is slightly larger than the jump rate obtained from MN measurements, $\tau_{\mathrm{MN}}^{-1} \approx 5 \times 10^4\ \mathrm{s}^{-1}$.

To deduce activation energies from the $R_{1\rho}(1/T)$ peaks and to gain information on the underlying dimensionality of the diffusion process, the rates were analyzed with an appropriate relaxation model introduced by Richards.[27,38]

The influence of x on the Li diffusivity can also be clearly rediscovered in the long-range activation energies E_a obtained from the appropriate fits that are shown in Figure 9a–c as solid lines. As is well-known for NMR relaxometry, the rate $R_{1\rho}$ is linked to the spectral density function $J(n\omega)_{n=1,2}$ via

$$R_{1\rho,\mathrm{diff}} = C_\rho\left(J(2\omega_1) + \frac{5}{3}J(\omega_0) + \frac{2}{3}J(2\omega_0)\right) \quad (3)$$

where ω_1 denotes the angular locking frequency, ω_0 the Lamor frequency and k_B the Boltzmann constant. Here, the spectral density function introduced by Richards[27] for 2D diffusion $J^{2D}(\omega,\tau_c) \propto \tau_c \ln(1 + 1/(1+ \omega_1\tau_c)^\beta)$ was used. It entails a logarithmic frequency dependence of the relaxation rate on the high-T side of the diffusion-induced rate peak. The rates were recorded at temperatures where the first term of eq 3 is sufficient to describe the relaxation rates adequately. Since the Li jump rate τ^{-1} is of the order of the correlation rate τ_c^{-1}, we obtain the following activation energies being characteristic for long-range ion transport that obeys the Arrhenius relation

$$\tau_c^{-1} \approx \tau_\rho^{-1} = \tau_0^{-1}\exp\left(\frac{-E_a^{2D}}{k_B T}\right) \quad (4)$$

The lowest activation energy E_a^{2D} of 0.44 eV is found for the sample with the lowest Li metal content ($x = 0.3$). A slightly higher energy of 0.48 eV is found for $x = 0.7$, while the highest activation energy of 0.65 eV is obtained for the fully intercalated sample with $x = 1$. This is in excellent agreement with the increase of $T_{\max}$ with increasing Li content x. The validity of the fits is supported by the results for the pre-exponential factor τ_0^{-1}, which is in the typical range of phonon frequencies;[50] here, we obtained $\tau_0^{-1} \approx 10^{13}...10^{15}\ \mathrm{s}^{-1}$.

Table 3. Results for the Pre-exponential Factor τ_0^{-1} and Activation Energies E_a

	$x = 0.3$	$x = 0.7$	$x = 1$
E_a^{2D}	0.44 eV	0.48 eV	0.65 eV
τ_0^{-1}	$3.44 \times 10^{13}\ \mathrm{s}^{-1}$	$1.96 \times 10^{13}\ \mathrm{s}^{-1}$	$4.28 \times 10^{15}\ \mathrm{s}^{-1}$

Let us note that it is good to know about the effective locking frequency used to carry out the fitting procedure. The fits shown here use the locking frequency that can be determined via the pulse power used to lock the spin system. The fact that for $x = 0.3$, a shallow R_1 maximum is seen, gives us the chance to use a joint fit to parametrize both the R_1 and $R_{1\rho}$ rates; by leaving the fitting parameter ω_1 free, we can estimate a value for $\omega_{\mathrm{effective}}$ that takes into account local fields. Here, it turned out that $\omega_{\mathrm{effective}}$ is only about 2–3 times larger than ω_1. This difference has almost no influence on the position and shape of the fits shown; its influence on the resulting E_A and the prefactor is quite small. Of course, the diffusion coefficient derived via the maximum condition is influenced by the same factor. Compared to other sources of error, this is quite small.

Using the fits shown in Figure 9a–c, the short-range activation energies E'_a, which describe the slope in the low-temperature limit $\omega_0\tau_c \gg 1$, can be easily estimated according to $E'^{2D}_a = E^{2D}_a \times (\beta - 1)$ with the correlation parameter β ($1 < \beta \leq 2$).[23,34,35] Interestingly, E'^{2D}_a behaves the other way round; the highest value (0.35 eV) is found for $x = 0.3$ ($\beta = 1.80$). Whereas for $x = 0.7$ ($\beta = 1.71$) an activation energy of 0.34 eV and for $x = 1$ ($\beta = 1.43$) the lowest value (0.28 eV) is found. Since E'^{2D}_a is governed by repulsive Coulomb interactions, its decrease with x (or the increase of β being a measure of these interactions) reflects Li–Li correlation effects rather than a reduction in local energy barriers. The larger the Li density, the more distinct correlated motion.[33,34] For $x = 0.3$, no large correlation effects are seen, since E'_a equals E^{2D}_a we assume that the Li ions are exposed to a regular, uniform potential landscape with almost no difference between short-range and long-range hopping motion, see also ref 50.

Moreover, frequency-dependent R_ρ measurements have been carried out at a constant temperature to differentiate between two-dimensional (2D) and three-dimensional (3D) diffusion, see Figure 10a.[20]

DOI: 10.1021/am5078655
ACS Appl. Mater. Interfaces 2015, 7, 4089–4099

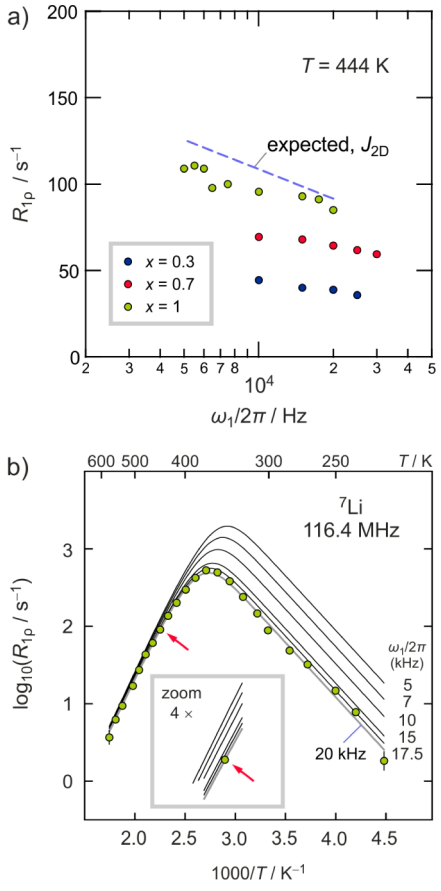

Figure 10. (a) ^{7}Li NMR $R\rho$ rates of 2H−Li_xNbS_2 as a function of the locking frequency $\omega_1/2\pi$. The frequency axis is scaled logarithmically. $R_{1\rho}$ was recorded at 444 K on the high-temperature flank of the relaxation rate peak where the condition $\omega_1\tau_1 \ll 1$ approximately holds. The solid line indicates the expected frequency dependence according to the semiempirical model for 2D diffusion by Richards ($R_{1\rho} \propto -\tau_c \ln(\omega_1\tau_c)$).[27] (b) Simulation of the expected frequency dependence for $Li_{1.0}NbS_2$ by varying the locking frequency from 5 to 20 kHz. As is visible in the inset a rather shallow dependence is expected at T = 444 K; the values predicted are in good agreement with those found experimentally.

In Figure 10b, the spectral density function $J^{2D}(\omega,\tau_c)$ (see above)[27] was used to calculate the expected frequency dependence $R_{1\rho,diff} \propto -\tau_c \ln(\omega_1\tau_c)$ of $Li_{1.0}NbS_2$ at 444 K (solid line), that is, within the high-temperature limit $\omega_1\tau_c \ll 1$.[38,51] Here, $R_{1\rho,diff}$ denotes the diffusion-induced R_ρ rate.[34] Most importantly, in contrast to 2D hopping motion, 3D diffusion would result in no frequency dependence of the $R_{1\rho,diff}$ rates in the limit $\omega_1\tau_c \ll 1$.[23] As it can be seen in the inset of Figure 10b, varying $\omega_1/2\pi$ in a rather small range, *viz* from 5 to 17 kHz only, needs highly precise R_ρ measurements to attest 2D diffusion in Li_xNbS_2. Despite of the narrow frequency range accessible via R_ρ NMR, the rates measured at 444 K indeed reveal a small frequency dependence being indicative of 2D diffusion. Comparing the present findings for the 2H-modification with previous measurements on 3R-$Li_{0.7}NbS_2$, it turned out, however, that the logarithmic frequency dependence is not as large as it was deduced from the frequency-dependent R_ρ measurements of the 3R-modification.[14] This difference might be due to differences in local crystal structure between the two polymorphs, especially when the connection of the LiS_6 and NbS_6 polyhedra is regarded (see above). Possibly, the free prismatic voids located above the LiS_6 octahedra in 2H−Li_xNbS_2 might lead to wavelike 2D diffusion, i.e., an oscillating trajectory which results if we consider sites within the van der Waals gap that act as transition states. Such transition states might be the tetrahedral sites connecting two octahedral voids by sharing common faces; a similar/please add semicolon after faces diffusion pathway has been found for Li_xTiS_2.[50,52,53]

Ultimately, although a characteristic 2D frequency dependence was found, we also fitted the diffusion-induced rate peak $R_{1\rho}$ by using the spectral density function developed for 3D diffusion introduced by Bloembergen, Purcell, and Pound (BPP).[36,37,54] In Figure 9b, the corresponding fit for the sample with x = 0.7 is shown as a dashed line. Since there is almost no difference between the 2D fit according to Richards (red line) and the 3D BPP fit (dashed line), without the frequency dependent measurements carried out here it would be very difficult to distinguish 2D from 3D motion just by analyzing the temperature dependence of $R_{1\rho}$. Most importantly, disregarding the dimensionality of the diffusion process, 3D fits generally lead to lower activation energies and prefactors τ_0^{-1}. Here, however, the logarithmic frequency dependence found serves as a good indication for 2D diffusion. This is strongly supported by the chemical shift anisotropy observed, which does not disappear with increasing temperature; thus even in the regime of fast Li motion the ions sense the spatially confined environment of the van der Waals gap. In line with this observation, no averaging or change of quadrupole intensities is seen at higher T. Consequently, to extract the correct activation energies E_a^{2D} the $R_{1\rho}(1/T)$ rate peaks have to be analyzed in terms of spectral density functions J^{2D} introduced for 2D jump diffusion.[27]

For the sake of completeness, a possible second $R_{1\rho}$ peak maximum for x = 1 has to be mentioned here (indicated as a dashed line in Figure 9c). Since no obvious second maximum was found for the other samples only the clearly observable rate peak was taken into account for the analysis of the samples studied.

Here, we found strong evidence for 2D diffusion, that is, Li^+ diffusion along the buried interfaces formed by the van der Waals gap of layer-structured Li_xNbS_2. For low Li contents, x = 0.3, Li diffusion turns out to be less influenced by correlation effects. In contrast to samples with larger values of x, activation energies from both R_L and R_ρ measurements (0.44 eV) indicate Li hopping within a regular potential landscape with almost no difference between short-range motion and long-range ion transport.

5. CONCLUSIONS

2H−Li_xNbS_2 turned out to be a suitable and intriguing model system with a layered structure to study both dimensionality effects in spatially confined dimensions as well as the influence of Li intercalation on local hopping and long-range ion transport. ^{7}Li NMR line shapes, as well as R_ρ measurements, have been used to get insights into both the Li ion dynamics and the geometry of Li motion in NbS_2.

(i) Frequency-dependent R_ρ measurements were successfully used to identify two-dimensional diffusion in 2H−Li_xNbS_2 taking place along the buried interfaces in the host material. The R_ρ rates of all samples show a small but clearly noticeable logarithmic frequency dependence within the high temperature limit characterized by $\omega_1\tau_c \ll 1$; the rates measured are in good agreement with the values expected for a 2D diffusion process if

DOI: 10.1021/am5078655
ACS Appl. Mater. Interfaces 2015, 7, 4089−4099

the semiempirical spectral density function introduced by Richards is used for the prediction. (ii) As has been shown via R_{ρ} NMR, the intercalation degree x influences Li ion diffusion in 2H−Li_xNbS_2 as expected. The larger x is chosen, the less the vacancy concentration, which slows down Li diffusivity in the van der Waals gap. This manifests itself in a characteristic shift of the rate $R_{1\rho}(1/T)$ peaks toward higher temperatures if x is increased from 0.3 to 1. Moreover, the slow-down of Li diffusivity is confirmed by a significant increase of the long-range activation energy that is raised from 0.44 (x = 0.3) to 0.64 eV (x = 1) if deduced from the fits for 2D jump diffusion, that is, Li ion diffusion along the inner van der Waals interface in NbS_2.

AUTHOR INFORMATION

Corresponding Author

*Webmail: bernhard.stanje@tugraz.at.

Notes

The authors declare no competing financial interest.

ACKNOWLEDGMENTS

We thank our colleagues at the TU Graz for valuable discussions; in particular, Dr. I. Hanzu for assistance with scanning electron microscopy. We thank the Deutsche Forschungsgemeinschaft (DFG) for financial support within the DFG Research Unit 1277 (subproject 1, WI 3600 2-2). Additional support from the Austrian Federal Ministry of Science, Research and Economy, and the Austrian National Foundation for Research, Technology and Development is also greatly appreciated.

REFERENCES

(1) Goodenough, J. B.; Park, K.-S. The Li-Ion Rechargeable Battery: A Perspective. *J. Am. Chem. Soc.* **2013**, *135*, 1167−1176.

(2) Whittingham, M. S. Lithium Batteries and Cathode Materials. *Chem. Rev.* **2004**, *104*, 4271−4302.

(3) Whittingham, M. Chemistry of Intercalation Compounds: Metal Guests in Chalcogenide Hosts. *Prog. Solid State Chem.* **1978**, *12*, 41−99.

(4) Wang, Q. H.; Kalantar-Zadeh, K.; Kis, A.; Coleman, J. N.; Strano, M. S. Electronics and Optoelectronics of Two-Dimensional Transition Metal Dichalcogenides. *Nat. Nanotechnol.* **2012**, *7*, 699−712.

(5) Ramakrishna Matte, H. S. S.; Gomathi, A.; Manna, A. K.; Late, D. J.; Datta, R.; Pati, S. K.; Rao, C. N. R. MoS_2 and WS_2 Analogues of Graphene. *Angew. Chem., Int. Ed.* **2010**, *49*, 4059−4062.

(6) Splendiani, A.; Sun, L.; Zhang, Y.; Li, T.; Kim, J.; Chim, C.-Y.; Galli, G.; Wang, F. Emerging Photoluminescence in Monolayer MoS_2. *Nano Lett.* **2010**, *10*, 1271−1275.

(7) Chhowalla, M.; Shin, H. S.; Eda, G.; Li, L.-J.; Loh, K. P.; Zhang, H. The Chemistry of Two-Dimensional Layered Transition Metal Dichalcogenide Nanosheets. *Nat. Chem.* **2013**, *5*, 263−275.

(8) Dahn, D.; Carolan, J.; Haering, R. Low-Temperature Specific Heat of Li_xNbS_2 Intercalation Compounds. *Phys. Rev. B* **1986**, *33*, 5214−5220.

(9) Kumagai, N.; Tanno, K.; Kumagai, N. Charge−Discharge Characteristics and Structural Change in Various Niobium Sulfide Cathodes for Lithium-Nonaqueous Secondary Batteries. *Electrochim. Acta* **1982**, *27*, 1087−1092.

(10) Liao, Y.; Park, K.-S.; Singh, P.; Li, W.; Goodenough, J. B. Reinvestigation of the Electrochemical Lithium Intercalation in 2H- and 3R-NbS_2. *J. Power Sources* **2014**, *245*, 27−32.

(11) Lévy, F. *Intercalated Layered Materials*; D. Reidel Publishing Company: Dordrecht, the Netherlands, 1979.

(12) Salyer, P. A.; Barker, M. G.; Gregory, D. H.; Jones, M. O.; Wilson, C. $Li_{0.7}NbS_2$: Structural Effects of Increased Alkali Metal Content. *Acta Crystallogr., Sect. E: Struct. Rep. Online* **2003**, *59*, i112−i115.

(13) Jellinek, F.; Brauer, G.; Müller, H. Molybdenum and Niobium Sulphides. *Nature* **1960**, *185*, 376−377.

(14) Epp, V.; Nakhal, S.; Lerch, M.; Wilkening, M. Two-Dimensional Diffusion in $Li_{0.7}NbS_2$ as Directly Probed by Frequency-Dependent ^{7}Li NMR. *J. Phys.: Condens. Matter* **2013**, *25*, 195402−1−7.

(15) Kuhn, A.; Narayanan, S.; Spencer, L.; Goward, G.; Thangadurai, V.; Wilkening, M. Li Self-Diffusion in Garnet-Type $Li_7La_3Zr_2O_{12}$ as Probed Directly by Diffusion-Induced ^{7}Li spin-Lattice Relaxation NMR Spectroscopy. *Phys. Rev. B* **2011**, *83*, 094302−1−11.

(16) Wilkening, M.; Küchler, W.; Heitjans, P. From Ultraslow to Fast Lithium Diffusion in the 2D Ion Conductor $Li_{0.7}TiS_2$ Probed Directly by Stimulated-Echo NMR and Nuclear Magnetic Relaxation. *Phys. Rev. Lett.* **2006**, *97*, No. 065901.

(17) McDowell, A.; Fedders, P.; Conradi, M. Spin Relaxation for Motion Restricted to Two Dimensions. *Phys. Rev. B* **1998**, *58*, 248−253.

(18) MacDonald, D. H.; Sholl, C. A.; Stephenson, P. C. L. Nuclear Magnetic Resonance Magnetic Dipolar Spectral Density Functions for Two-Dimensional Lattice Diffusion: Hexagonal Systems. *J. Phys.: Condens. Matter* **1998**, *10*, 417−428.

(19) Wilkening, M.; Heitjans, P. From Micro to Macro: Access to Long-Range Li^+ Diffusion Parameters in Solids via Microscopic ^{6}, ^{7}Li Spin-Alignment Echo NMR Spectroscopy. *ChemPhysChem* **2012**, *13*, 53−65.

(20) McDowell, A.; Mendelsohn, C.; Conradi, M.; Bowman, R.; Maeland, A. Two-Dimensional Diffusion of Hydrogen in $ZrBe_2H_{1.4}$. *Phys. Rev. B* **1995**, *51*, 6336−6342.

(21) Epp, V.; Wilkening, M. Fast Li Diffusion in Crystalline $LiBH_4$ Due to Reduced Dimensionality: Frequency-Dependent NMR Spectroscopy. *Phys. Rev. B* **2010**, *82*, No. 020301.

(22) Kuhn, A.; Sreeraj, P.; Pöttgen, R.; Wiemhöfer, H.-D.; Wilkening, M.; Heitjans, P. Li Ion Diffusion in the Anode Material $Li_{12}Si_7$: Ultrafast Quasi-1D Diffusion and Two Distinct Fast 3D Jump Processes Separately Revealed by ^{7}Li NMR Relaxometry. *J. Am. Chem. Soc.* **2011**, *133*, 11018−11021.

(23) Heitjans, P.; Schirmer, A.; Indris, S. In *Diffusion in Condensed Matter*; Heitjans, P., Kärger, J., Eds.; Springer: Berlin, 2005; pp 367−415.

(24) Epp, V.; Wilkening, M. Motion of Li^+ in Nanoengineered $LiBH_4$ and $LiBH_4$:Al_2O_3 Comparison with the Microcrystalline Form. *ChemPhysChem* **2013**, *14*, 3706−3713.

(25) Wilkening, M.; Amade, R.; Iwaniak, W.; Heitjans, P. Ultraslow Li Diffusion in Spinel-Type Structured $Li_4Ti_5O_{12}$—A Comparison of Results from Solid State NMR and Impedance Spectroscopy. *Phys. Chem. Chem. Phys.* **2007**, *9*, 1239−1246.

(26) Wilkening, M.; Kuhn, A.; Heitjans, P. Atomic-Scale Measurement of Ultraslow Li Motions in Glassy $LiAlSi_2O_6$ by Two-Time ^{6}Li Spin-Alignment Echo NMR Correlation Spectroscopy. *Phys. Rev. B* **2008**, *78*, No. 054303.

(27) Richards, P. M. In *Topics in Current Physics*; Salamon, M. B., Ed.; Springer: Berlin, 1979; pp 141−174.

(28) Rodriguez-Carvajal, J. FULLPROF: A Program for Rietveld Refinement and Pattern Matching Analysis. *Abstr. Satell. Meet. Powder Diffr. XV Congr. IUCr* **1990**, 127.

(29) Fukushima, E.; Roeder, S. B. W. *Experimental Pulse NMR: A Nuts and Bolts Approach*; Perseus Books, Advanced Book Program: Reading, MA, 1981.

(30) Ailion, D.; Slichter, C. Observation of Ultra-Slow Translational Diffusion in Metallic Lithium by Magnetic Resonance. *Phys. Rev.* **1965**, *137*, A235−A245.

(31) Look, D. C. Nuclear Magnetic Dipole−Dipole Relaxation Along the Static and Rotating Magnetic Fields: Application to Gypsum. *J. Chem. Phys.* **1966**, *44*, 2995−3000.

(32) Redfield, A. Nuclear Magnetic Resonance Saturation and Rotary Saturation in Solids. *Phys. Rev.* **1955**, *98*, 1787−1809.

DOI: 10.1021/am5078655
ACS Appl. Mater. Interfaces 2015, 7, 4089−4099

(33) Meyer, M.; Maass, P.; Bunde, A. Spin-Lattice Relaxation: Non-Bloembergen-Purcell-Pound Behavior by Structural Disorder and Coulomb Interactions. *Phys. Rev. Lett.* **1993**, *71*, 573−576.
(34) Bunde, A., Dieterich, W., Maass, P., Meyer, M. In *Diffusion in Condensed Matter—Methods, Materials, Models*, 2nd ed.; Heitjans, P., Kärger, J., Eds.; Springer: Berlin, 2005; pp 813−856.
(35) Funke, K. Jump Relaxation in Solid Electrolytes. *Prog. Solid State Chem.* **1993**, *22*, 111−195.
(36) Bloembergen, N.; Purcell, E.; Pound, R. Relaxation Effects in Nuclear Magnetic Resonance Absorption. *Phys. Rev.* **1948**, *73*, 679−712.
(37) Küchler, W.; Heitjans, P.; Payer, A.; Schollhorn, R. ^{7}Li NMR Relaxation by Diffusion in Hexagonal and Cubic Li_xTiS_2. *Solid State Ionics* **1994**, *70−71*, 434−438.
(38) Richards, P. M. Effect of Low Dimensionality on Prefactor Anomalies in Superionic Conductors. *Solid State Commun.* **1978**, *25*, 1019−1021.
(39) Omloo, W.; Jellinek, F. Intercalation Compounds of Alkali Metals with Niobium and Tantalum Dichalcogenides. *J. Less-Common Met.* **1970**, *20*, 121−129.
(40) Abragam, A. *The Principles of Nuclear Magnetism*; Clarendon Press: Oxford, U.K., 1961.
(41) Bredow, T.; Heitjans, P.; Wilkening, M. Electric Field Gradient Calculations for Li_xTiS_2 and Comparison with ^{7}Li NMR Results. *Phys. Rev. B* **2004**, *70*, No. 115111.
(42) Prigge, C.; Müller-Warmuth, W.; Schöllhorn, R. NMR Studies of Lithium Intercalated in the Host Compounds 1T-TiS_2, c-TiS_2 and VSe_2. *Z. Phys. Chem.* **1995**, *189*, 153−168.
(43) Wilkening, M.; Epp, V.; Feldhoff, A.; Heitjans, P. Tuning the Li Diffusivity of Poor Ionic Conductors by Mechanical Treatment: High Li Conductivity of Strongly Defective $LiTaO_3$ Nanoparticles. *J. Phys. Chem. C* **2008**, *112*, 9291−9300.
(44) Ailion, D.; Slichter, C. Study of Ultraslow Atomic Motions by Magnetic Resonance. *Phys. Rev. Lett.* **1964**, *12*, 168−171.
(45) Slichter, C.; Ailion, D. Low-Field Relaxation and the Study of Ultraslow Atomic Motions by Magnetic Resonance. *Phys. Rev.* **1964**, *135*, A1099−A1110.
(46) Wolf, D. Effect of Correlated Self-Diffusion on the Low-Field Nuclear-Spin Relaxation in the Rotating Reference Frame. *Phys. Rev. B* **1974**, *10*, 2724−2732.
(47) Epp, V.; Gün, Ö.; Deiseroth, H.-J.; Wilkening, M. Long-Range Li^+ Dynamics in the Lithium Argyrodite Li_7PSe_6 as Probed by Rotating-Frame Spin−Lattice Relaxation NMR. *Phys. Chem. Chem. Phys.* **2013**, *15*, 7123−2132.
(48) Hubbard, P. Nonexponential Nuclear Magnetic Relaxation by Quadrupole Interactions. *J. Chem. Phys.* **1970**, *53*, 985−987.
(49) Tse, D.; Hartmann, S. Nuclear Spin-Lattice Relaxation via Paramagnetic Centers without Spin Diffusion. *Phys. Rev. Lett.* **1968**, *21*, 511−514.
(50) Wilkening, M.; Heitjans, P. Li Jump Process in *h*-$Li_{0.7}TiS_2$ Studied by Two-Time ^{7}Li Spin-Alignment Echo NMR and Comparison with Results on Two-Dimensional Diffusion from Nuclear Magnetic Relaxation. *Phys. Rev. B* **2008**, *77*, No. 024311.
(51) Avogadro, A.; Villa, M. Nuclear Magnetic Resonance in a Two-Dimensional System. *J. Chem. Phys.* **1977**, *66*, 2359−2367.
(52) Bensch, W.; Bredow, T.; Ebert, H.; Heitjans, P.; Indris, S.; Mankovsky, S.; Wilkening, M. Li Intercalation and Anion/Cation Substitution of Transition Metal Chalcogenides: Effects on Crystal Structure, Microstructure, Magnetic Properties, and Li^+ Ion Mobility. *Prog. Solid State Chem.* **2009**, *37*, 206−225.
(53) Van der Ven, A.; Thomas, J.; Xu, Q.; Swoboda, B.; Morgan, D. Nondilute Diffusion from First Principles: Li Diffusion in Li_xTiS_2. *Phys. Rev. B: Condens. Matter Mater. Phys.* **2008**, *78*, No. 104306.
(54) Böhmer, R.; Jeffrey, K. R.; Vogel, M. Solid-State Li NMR with Applications to the Translational Dynamics in Ion Conductors. *Prog. Nucl. Magn. Reson. Spectrosc.* **2007**, *50*, 87−174.

DOI: 10.1021/am5078655
ACS Appl. Mater. Interfaces 2015, 7, 4089−4099